

Self-similar dynamics of air film entrained by a solid disk in confined space: a simple prototype of topological transitions

Hana Nakazato, Yuki Yamagishi, and Ko Okumura

Physics Department, Faculty of Science, Ochanomizu University

(Dated: November 9, 2018)

Abstract

In hydrodynamic topological transitions, one mass of fluid breaks into two or two merge into one. For example, in the honey-drop formation when honey dripping from a spoon, honey is extended to separate into two as the liquid neck bridging them thins down to micron scales. At the moment when topology changes due to the breakup, physical observables such as surface curvature locally diverges. Such singular dynamics have widely attracted physicists, revealing universality in their self-similar dynamics, which share much in common with critical phenomena in thermodynamics. Many experimental examples have been found, which include electric spout and vibration-induced jet eruption. However, only a few cases have been physically understood on the basis of equations that govern the singular dynamics and even in such a case the physical understanding is mathematically complicated inevitably involving delicate numerical calculations. Here, we study breakup of air film entrained by a solid disk into viscous liquid in a confined space, which leads to formation, thinning and breakup of the neck of air. As a result, we unexpectedly find that equations governing the neck dynamics can be solved analytically by virtue of two remarkable experimental features: only a single length scale linearly dependent on time remains near the singularity and universal scaling functions describing singular neck shape and velocity field are both analytic. The present solvable case would be essential for our better understanding of the singular dynamics and will help unveil the physics of unresolved examples intimately related to daily-life phenomena and diverse practical applications.

The self-similar dynamics in hydrodynamics was already on focus in 1982, when the dynamics of viscous instability of a moving front was studied [1] and the renormalization group theory in statistical physics, which elucidates universality appearing in critical phenomena in thermodynamics, was recognized worldwide beyond fields [2]. In 1993, the self-similar dynamics was first studied for breakup of droplets (capillary pinch-off) [3], one typical example of topological transitions. In the seminal paper, the scaling ansatz, one of the key ideas leading to universality in critical phenomena, was shown to be useful. This paper ignited a surge of publication on the self-similarity in fluid breakup phenomena in 1993 and 1994 [4–7]

In 1999, analytical solution for the dynamics of droplet coalescence, another typical example of hydrodynamic topological transitions, was published [8]. This is followed by many studies on the dynamics of droplets and bubbles, such as coalescence [9–13], non-coalescence [14], pinch-off [15, 16], and droplet impact onto substrates [17–22], with a rapid technological advance in high-speed imaging and numerical computing. However, since then, the field has rather remotely been developed from the self-similar dynamics, while one of the main foci has been on simple scaling laws [23], which is another key concept in understanding universality in critical phenomena.

Up to date, many types of singular transitions, which is more general than topological transitions, and associated self-similar dynamics have been found experimentally in hydrodynamics. Such singular transitions often exhibit universality via self-similar dynamics near the singular point, while non-universal behavior is observed under certain conditions [24]. Other examples often related to practical applications include spout of liquid jet under electric field [25] (closely related to ink-jet printing) and jet eruption under vibration [26]. In addition, the self-similar dynamics was found for the first time in droplet coalescence under electric field [27] (relevant to microfluidic applications). Self-similarities are sometimes identified not only in the dynamics as in the above examples but also in the steady-state flow towards singular transitions, in which topology is not necessarily changed, as observed in flow-induced air entrainment [28–30] and selective withdrawal [31]; both of them are useful, e.g., for macroscopic [32] and microscopic coatings [33] important for chemical, biological, and medical engineering.

As indicated above, each example of singular transitions is often familiar to everyone and/or important for applications. In fact, our example of fluid breakup is central to di-

verse processes, involving two-phase flows, emulsification and drop formation, in industrial, engineering, and scientific realms. Understanding physical laws governing the dynamics is useful for various purposes [34]: e.g., (1) industrial production of food such as mayonnaises and cream and of spray system for painting or planting, (2) engineering development of microfluidic devices promising for applications in chemistry, biochemistry and material science, and (3) atmospheric science dealing with formation of raindrops and thunderstorms.

As for the emergence of universality, singular transitions are analogous to critical phenomena in thermodynamic transitions [35–37]. By identifying characteristic physical quantities and lengths describing the fluid dynamics near the singularity, the properties of the interface and the flow can be understood in terms of a similarity solution near the transition point, which allows a simplified description of the dynamics, leading to a deeper understanding of the phenomena.

However, only a few examples of the above-mentioned singular dynamics have been understood, and even if well understood, the theory is intricate involving delicate numerical calculations (In contrast, universal dynamics associated with hydrodynamic instability have been rather simply understood [1, 38]). Because of this, understanding of the singular dynamics is premature. If otherwise, as has been done for critical phenomena, universalities for the singular dynamics could have been classified.

Here, we report an experimental and theoretical study of appearance of a singularity by air entrainment caused by a solid disk into a confined viscous medium in the Hele-Shaw cell. The remarkable features of the present case are that only a single length scale remains near the singularity to characterize the dynamics and that the length scale simply scales linearly with time. These exceptionally simple characteristics make the theory completely solvable in a perturbative sense, leading to analytic scaling functions and demonstrating the essential physical mechanisms of the singular dynamics in a clear way. Most of previous experimental examples possess more than one remaining length scales near the singularity and at least one of universal scaling functions is nonanalytic. This is indeed the case for well-understood cases [7] such as the pioneering study associated with the Hele-Shaw cell [3] (see just below Eq.(7)) and another seemingly similar case of the flow-induced air entrainment [28, 30] (see Discussion for details). Accordingly, the present study advances our general understanding of the singular dynamics; it represents an important fundamental example of the singular dynamics, providing insight into unresolved self-similar dynamics such as the electric spout

of liquid [25], the selective withdrawal [31], and the electric-field-induced drop coalescence [27], and impacting onto the study of the dynamics of droplets and bubbles in general.

I. RESULTS

A. Experimental

The experimental setup is shown in Fig. 1(a). We create a Hele-Shaw cell with the thickness D , and fill the cell with a viscous oil (polydimethylsiloxane, or PDMS) with the kinematic viscosity $\nu = \eta/\rho$ where η and ρ are the viscosity and density of the oil. We insert a stainless disk [the radius R , the thickness D_0 ($< D$), the density ρ_s] at the top of the cell. The bottom of the disk touches the liquid-air interface with zero velocity and the disk starts to go down in the oil phase due to gravity. Since the disk thickness is slightly thinner than the cell thickness D , the disk does not directly touch the cell plates and a thin layer of oil is formed between a front cell plate and a front surface of the disk. The thickness of the film e is fixed to the value $e = (D - D_0)/2$ (Fig. 1(b)). As a result, the air is dragged by the disk as in Fig. 1(c) forming a singular shape, with details revealed in Fig. 2(a) and (b) (see movies 1 to 4 [39]), and finally pinches off to cause a topological transition.

The (x, y, z) coordinate system is specified in Fig. 2(c) (see also Fig. 1(c) in which the center of gravity of the disk is denoted by z_G). For simplicity, the space-time position at the critical moment of pinch-off $(t, x, z) = (t_c, x_c, z_c)$ is set to the origin of the (t, x, y) coordinate if not specified. The right-hand side of the air-liquid surface is described by $x = h(t, z)$. The minimum of the function $h(t, z)$ as a function of z is denoted as $(x, z) = (h_m, z_m)$. Under our experimental conditions, the shape of the neck is not axisymmetric and is rather independent from the y coordinate. In fact, as shown in the magnified snapshot in Fig. 2(a) and (b), the singular neck shape near the pinch-point is like a sheet of thickness $2h_m$ and width $\simeq D_0$.

Now, we discuss experimental details of the experiment. The height and width of Hele-Shaw cells are 12 cm and 9 cm, respectively. The two plates are separated by a spacer of thickness D . To make the thickness of two thin film layers formed on both sides of the disk to be nearly equal, we attach two small acrylic plates at the inside surfaces of the cell plates near the top of the cell. The thickness of the small plates are slightly smaller than e and the

attached two plates play a role of a gate for the inserted disk. In the present experiment, we examined different values of e ($= 0.2, 0.5$, and 1.0 mm) and confirmed that the results are independent of the value of e in the range. The disk is pre-wetted by the oil before being dropped into the cell; there is no contact line on the surface of the disk, which removes any effects of the contact angle on the phenomena. When the cell thickness is smaller than the values (3 to 5 mm) studied in the present study, the falling velocity of the disk becomes significantly smaller; there seems to be another regime, in which the cavity shape near the contact with the disk becomes cone-like, unlike the present regime characterized by the sheet formation; this issue will be discussed elsewhere. We used a high-speed camera (Fastcam SA-X, Photron) with a macro lens (Micro NIKKOR 60 mm f2.8G ED, Nikon) and analyzed images with a software (Image J). The density of stainless steel (SUS430) is 7.7 g/cm^3 , while that of PDMS depends on viscosity: 0.965 for 100 cS and 0.97 for 500 and 1000 cS and 0.975 for 10000 cS in the unit g/cm^3 .

B. Dynamics of the neck

Figures 3(a)-(b) show z_m and h_m , together z_G , as a function of time for various parameters ν , D , and R ($e = 0.5$ mm). Figure 3(c) clearly shows the following relations:

$$2h_m = z_m = z_G \equiv l(t) \quad (1)$$

where $l(t)$ ($t < 0$) is given by

$$l(t) \equiv v_0 \times (-t) \quad \text{where } v_0 = k \frac{\Delta \rho g D^2}{\eta} \quad (2)$$

with $k = 0.02764 \pm 0.00008$, which is close to $1/(12\pi) \simeq 0.0265$, and $\Delta \rho = \rho_s - \rho$ (see Discussion for the expression for v_0).

Plots in Fig. 4(a)-(c) demonstrate, for two different parameter sets, that the neck profile $h(t, z)$ has the following scaling form, demonstrating a self similar dynamics with the single length scale $l(t)$:

$$2h(t, z)/l(t) = H(z/l(t)) \quad (3)$$

Figure 4(d) shows that the data agree quite well with the expression

$$H(\xi) = 1 + a(\xi - 1)^2 \text{ with } \xi = z/l \quad (4)$$

with $a = 3.1415 \pm 0.011$, which is close to π . As stated above, remaining of only a single length scale near singularity is an exceptionally simple case, similar to the coalescence case [27], for which physical understanding is lacking.

Further details are discussed below. Since the liquid completely wet the cell plates, we measure the inner edge of the neck image as $2h$. In Fig. 3a and b, the dashed line (the guide for the eye) are drawn by fitting the first three data (excluding the data at $t = 0$) for z_G (or z_m if z_G is not available). In Fig. 4c and d, the average of the left and right branches are used for the analysis to reduce the experimental error.

C. Theory

As shown below, the existence of the self-similar solution in Eq. (3) with its asymptotic form in Eq. (4) and the linear dependence of $l(t)$ on t in Eq. (2) can be explained by considering the air flow near the neck. Below, the physically most important component of the flow, i.e., the z direction, v_z , is denoted as v . Considering that a sheet of air with thickness $\simeq 2h$ (and width in the y direction $\simeq D_0$ slightly smaller than D) is formed near the neck, as seen in Fig. 2(a) and (b), it is reasonable to assume that v is independent of y near $y = 0$ because $h \ll D$. ($y = 0$ corresponds to the central position between the two walls separated by the distance D .) We can further assume that v is independent of x , i.e., $v = v_z(t, z)$, near the pinch-off point. This is because the narrowest point of the neck located at $z = z_m = l(t) = -v_0 t$ moves downwards with the velocity v_0 (> 0), and thus the liquid-air interface drags downwards air at the interface, which makes a plug flow inside the air neck, since Reynolds number $\text{Re} = \rho_a v_0 h / \eta_a$ approaches infinitely small towards the singular point ($\rho_a \simeq 1 \text{ kg/m}^3$ and $\eta_a \simeq 10^{-5} \text{ Pa}\cdot\text{s}$ are the density and viscosity of air and $\text{Re} < 0.1$ for $h < 1 \text{ mm}$ since $v_0 < 10^{-3} \text{ m/s}$). Now that we have shown the independence of v from x and y near the singularity, we obtain the following condition

$$v(t, z = z_m) = -v_0, \quad (5)$$

and the following equation of continuity:

$$\frac{\partial h}{\partial t} + \frac{\partial hv}{\partial z} = 0. \quad (6)$$

Eq. (6) can also be justified in the following manner. The pressure value at the neck is almost precisely equal to that of the atmospheric pressure $p_0 \simeq 10^5$ Pa, which implies $\partial \rho_a / \partial t = 0$ (with the air density ρ_a) even for a thin neck. This is because Laplace's pressure jump Δp is negligible compared with p_0 as long as the radius of curvature of the air liquid interface is larger than 0.01 mm, which is the present case; since the neck forms a sheet, the radius of curvature is independent of the width of a neck. This is in contrast with the axisymmetric case, in which the radius of curvature scales as the thin neck width and thus the pressure jump becomes significant at the neck.

Dynamics of h and v coupled in Eq. (6) is completely specified by introducing one more equation: the z component of the Navier-Stokes equation in the small h limit, in which viscosity dominates inertia (note that $\partial_x v_z = 0$ as before):

$$\eta_a \frac{\partial^2 v}{\partial z^2} = \frac{\partial \Delta p}{\partial z} \text{ with } \Delta p = -\gamma \frac{\partial^2 h}{\partial z^2}. \quad (7)$$

(Here, γ is the surface tension of the liquid.) In the pioneering study [3], the left-hand side of this equation is replaced by an averaged Poiseuille flow independent of z , which unexpectedly leads to a much more complicated scenario for the appearance of universality.

Eq. (7) can also be justified in the following manner, i.e., we can confirm retrospectively that the dominating terms in the z component of the Navier-Stokes equation is indeed expressed as in Eq. (7) near the singularity. From the experimental results, near the singular point, we expect characteristic scales in the x and z directions l_x and l_z and a characteristic time scale τ can be given by $l_x = l_z = \varepsilon l_0$, and $\tau = \varepsilon t_0$ with introducing a small dimensionless parameter ε and units of length and time, l_0 and t_0 , which is explained as follows. Since the experiment suggests that there is only a single length scale near the singularity, we can set $l_x = l_y = \varepsilon l_0$. The velocity in the z direction is characterized by v_0 , a finite value independent of ε . This implies the characteristic time scale t_c for the problem is given by $\tau = \varepsilon t_0$ because $v_0 \simeq l_x / \tau \simeq l_y / \tau$ is independent of ε . We can now estimate the order of each term in the z component of the Navier-Stokes equation. The inertial terms

$\rho_a(\partial_t v_z + v_x \partial_x v_z + v_z \partial_z v_z)$ scale as ε^{-1} and the gravitational term $\rho_a g$ scale as ε^0 , and the terms remaining in Eq. (7) all scale as ε^{-2} , which justifies that Eq. (7) properly collects relevant leading order terms near the singularity where $\varepsilon \approx 0$.

We employ the scaling ansatzs [3, 4, 6, 7, 24, 40]

$$2h(t, z) = z_0 \tilde{t}^\alpha H(\tilde{z}/\tilde{t}^\beta); \quad v(t, z) = -v'_0 \tilde{t}^\gamma V(\tilde{z}/\tilde{t}^\delta) \quad (8)$$

with introducing dimensionless scaling function H and V along with the dimensionless variables $\tilde{z} = (z - z_c)/z_0 = z/z_0$ and $\tilde{t} = v'_0(t_c - t)/z_0 = (-v'_0 t)/z_0$ where z_0 and v'_0 are arbitrary length and velocity scales, respectively, and substitute them into Eqs. (6) and (7). (Note in Eq. (8) that γ denotes a dimensionless exponent, not the surface tension.) We here require that the ansatzs are relevant for these equations near the singularity where $\tilde{t} \approx 0$ (i.e., equating all the exponents for the variable \tilde{t}) to obtain $\alpha = \beta = \delta = 1$ and $\gamma = 0$. This set reproduces (with the identification $v_0 = v'_0$) the scaling form in Eq. (3) and reveals another scaling structure,

$$v(t, z) = -v_0 V(z/l(t)) \quad (9)$$

In other words, the present analysis concludes that there is only a single length scale $l(t)$ near the singularity as observed in experiment, which linearly scales with t .

Substitution of the scaling forms in Eqs. (3) and (9), thus obtained theoretically, into Eq. (6) makes the variables t and $\xi = z/l$ to be separated: the original partial differential equation can be changed into a set of ordinary differential equations (the first equation confirms the linear t -dependence of $l(t)$; see the next paragraph for details):

$$dl/dt = -v_0 \quad (10)$$

$$(HV)' = \xi H' - H \quad (11)$$

Here, H and V are a function of ξ and the prime indicates the derivative with respect to ξ . The same substitution into Eq. (7) results in the following expression:

$$V'' = \lambda H''' \quad \text{with } \lambda = -\gamma/(2\eta v_0) \quad (12)$$

Equations (11) and (12) should satisfy the following boundary conditions (see Fig. 4 for the first two and Eq. (5) for the last):

$$H(1) = 1, H'(1) = 0, V(1) = 1 \quad (13)$$

Instead of starting from the general ansatz in Eq. (8), we can start directly from the scaling ansatz in Eqs. (3) and (9), motivated by experimental results, without assuming the linear t -dependence of $l(t)$ (with accepting the existence of a single length scale near the singularity as an experimental fact). From this standpoint, we can show from Eq. (10) that $l(t)$ should be linearly dependent on t , and we can explain the asymptotic form of the self similar shape in Eq. (4).

To our surprise, the boundary problem defined by the two ordinary differential equations for H and V in Eqs. (11) and (12) with the boundary conditions in Eq. (13) can be solved perturbatively as explained in the next paragraph. By assuming the series expansion $H(\xi) = a_0 + a_1\zeta + a_2\zeta^2 + \dots$ with $\zeta = \xi - 1$, we can show $a_0 = 1$, $a_1 = 0$, $a_2 = 3\lambda a_4$, $a_3 = 0, \dots$, i.e., for $\zeta \ll 1$

$$H(\xi) = 1 + a_2\zeta^2 + \dots, \text{ and } V(\xi) = 1 - \zeta + \dots, \quad (14)$$

which explains the experimental result including Eq. (4). Note that we can show $a_n = 0$ for odd n and we can derive expression for a_n as a function of a_m (with $m < n$) for even n up to any desired order: the present boundary problem can be solved completely in a perturbative sense. As far as we know, there have been no previous examples of hydrodynamic singular transition in which scaling functions for the shape and velocity (H and V) are both analytic; in all the previously known examples, at least one of the scaling functions is nonanalytic.

Now we derive Eq. (14). Equation (11) can be rearranged as

$$(1 + V')H = (\xi - V)H', \quad (15)$$

from which we obtain

$$\frac{dH}{H} = f(\xi)d\xi \text{ with } f(\xi) = \frac{1 + V'}{\xi - V} \quad (16)$$

By using the boundary condition $H(1) = 1$, we get

$$H(\xi) = e^{F(\xi)} \text{ with } F(\xi) = \int_1^\xi f(\xi) d\xi \quad (17)$$

Since the definition of $f(\xi)$ in Eq. (16) can be recast into the form

$$V' + f(\xi)V = \xi f(\xi) - 1, \quad (18)$$

This first-order linear differential equation for V can be solved as

$$V(\xi) = e^{-F(\xi)} \left[\int_1^\xi d\tilde{\xi} e^{F(\tilde{\xi})} \left\{ \tilde{\xi} f(\tilde{\xi}) - 1 \right\} + 1 \right], \quad (19)$$

which satisfies $V(1) = 1$. With using Eq. (17), we get

$$V(\xi) = \frac{1}{H} \left[\int_1^\xi d\tilde{\xi} H \left\{ \tilde{\xi} \frac{H'}{H} - 1 \right\} + 1 \right] \quad (20)$$

$$= \xi - 2 \int_1^\xi d\tilde{\xi} H(\tilde{\xi})/H(\xi) \quad (21)$$

From the conditions $H(1) = 1$ and $H'(1) = 0$, we expand $H(\xi)$ as

$$H(\xi) = 1 + a_2 \zeta^2 + a_3 \zeta^3 + a_4 \zeta^4 + \dots \quad (22)$$

with $\zeta = \xi - 1$. From this we obtain

$$V(\xi) = \xi - 2\zeta \frac{1 + a_2 \zeta^2/3 + a_3 \zeta^3/4 + a_4 \zeta^4/5 + \dots}{1 + a_2 \zeta^2 + a_3 \zeta^3 + a_4 \zeta^4 + \dots} \quad (23)$$

$$= 1 - \zeta + 2\zeta(2a_2 \zeta^2/3 + 3a_3 \zeta^3/4 - (2a_2^2/3 - 4a_4/5)\zeta^4 + \dots) \quad (24)$$

Substituting Eqs. (22) and (23) into Eq. (12), we can determine a_n perturbatively as a function of a_m (with $m < n$) to obtain Eq. (14).

II. DISCUSSION

Among the previous studies of singular transitions, the present problem may be very similar to air entrainment induced by flow [28, 30] in that (1) this singularity occurs for air surrounded by viscous liquid and (2) a thin sheet of air is formed so that the problem is two-dimensional but lacks axial symmetry. However, there is an essential difference: the present self-similarity is for the dynamics, while the self-similarity discussed for the flow-induced air entrainment is for the steady-state flow approaching a transition. In fact, the universal scaling function for the shape in the previous study cannot be expressed as a Taylor series expansion but needs a Frobenius series with a singular exponent $3/2$.

We can further explain why v_0 is given by the second expression in Eq. (2). For this purpose, we note that v_0 is the magnitude of falling velocity U ($= dz_G/dt$) of the disk in the oil phase, as seen from Eqs. (1) and (2). The falling velocity U could be determined by the balance between the gravitational energy gain $\Delta\rho g R^2 D_0 U$ per time and an appropriate viscous dissipation, which should be the most dominant one among the following three [41]: dissipation associated with the Couette flow developed inside thin films between the disk surface and the cell wall $\simeq \eta(U/e)^2 R^2 e$ and dissipations associated with Poiseuille flows around the disk corresponding to the velocity gradient in the y direction $\simeq \eta(U/D)^2 R^2 D$ and in the radial direction for the disk $\simeq \eta(U/R)^2 R^2 D$. The last dissipation may be smaller than the first two because $e, D \ll R$. However, the relative importance of the first and second is delicate; while the volume of dissipation for the first is well described by $2\pi R^2 D$, that for the second can be $\pi(cR)^2 D$ with a fairly large numerical constant c . In the present case, c seems indeed fairly large and the second dissipation seems the most dominant. This is because the balance of this dissipation and the gravitational energy gain gives $U \simeq \Delta\rho g D^2/\eta$, which is consistent with Eq. (2).

In summary, our theoretical result explains experimental findings, starting from the governing equations in (6) and (7); by virtue of the ansatzs in Eq. (8), we showed that only a single length scale remains near the singularity and this length linearly scales with t , and we further explained why we observed the self similar shape dynamics demonstrated in Fig. 4 and represented by Eqs. (3) and (4).

Acknowledgments

This work was partly supported by Grant-in-Aid for Scientific Research (A) (No. 24244066) of JSPS, Japan, and by ImPACT Program of Council for Science, Technology and Innovation (Cabinet Office, Government of Japan).

- [1] Huppert, H. E. Flow and instability of a viscous current down a slope. *Nature* **300**, 427–429 (1982).
- [2] Wilson, K. G. The renormalization group and critical phenomena. *Reviews of Modern Physics* **55**, 583 (1983).
- [3] Constantin, P. *et al.* Droplet breakup in a model of the hele-shaw cell. *Phys. Rev. E* **47**, 4169–4181 (1993).
- [4] Eggers, J. Universal pinching of 3d axisymmetric free-surface flow. *Phys. Rev. Lett.* **71**, 3458 (1993).
- [5] Goldstein, R. E., Pesci, A. I. & Shelley, M. J. Topology transitions and singularities in viscous flows. *Physical Review Letters* **70**, 3043 (1993).
- [6] Shi, X., Brenner, M. & Nagel, S. A cascade of structure in a drop falling from a faucet. *Science* **265**, 219 (1994).
- [7] Eggers, J. Nonlinear dynamics and breakup of free-surface flows. *Rev. Mod. Phys.* **69**, 865–930 (1997).
- [8] Eggers, J., Lister, J. & Stone, H. Coalescence of liquid drops. *J. Fluid Mech.* **401**, 293–310 (1999).
- [9] Aarts, D. G. A. L., Lekkerkerker, H. N. W., Guo, H., Wegdam, G. H. & Bonn, D. Hydrodynamics of droplet coalescence. *Phys. Rev. Lett.* **95**, 164503 (2005).
- [10] Burton, J. C. & Taborek, P. Role of dimensionality and axisymmetry in fluid pinch-off and coalescence. *Phys. Rev. Lett.* **98**, 224502 (2007).
- [11] Paulsen, J. D. *et al.* The inexorable resistance of inertia determines the initial regime of drop coalescence. *Proceedings of the National Academy of Sciences* **109**, 6857–6861 (2012).
- [12] Paulsen, J. D., Carmigniani, R., Kannan, A., Burton, J. C. & Nagel, S. R. Coalescence of bubbles and drops in an outer fluid. *Nature communications* **5**, 3182 (2014).

- [13] Paulsen, J. D., Carmigniani, R., Kannan, A., Burton, J. C. & Nagel, S. R. Coalescence of bubbles and drops in an outer fluid. *Nature Commun.* **5** (2014).
- [14] Ristenpart, W. D., Bird, J. C., Belmonte, A., Dollar, F. & Stone, H. A. Non-coalescence of oppositely charged drops. *Nature* **461**, 377–380 (2009).
- [15] Burton, J., Rutledge, J. & Taborek, P. Fluid pinch-off dynamics at nanometer length scales. *Physical review letters* **92**, 244505 (2004).
- [16] Burton, J. & Taborek, P. Bifurcation from bubble to droplet behavior in inviscid pinch-off. *Physical review letters* **101**, 214502 (2008).
- [17] Richard, D., Clanet, C. & Quéré, D. Surface phenomena: Contact time of a bouncing drop. *Nature* **417**, 811– (2002).
- [18] Okumura, K., Chevy, F., Richard, D., Quéré, D. & Clanet, C. Water spring: A model for bouncing drops. *EPL (Europhysics Letters)* **62**, 237 (2003).
- [19] Xu, L., Zhang, W. W. & Nagel, S. R. Drop splashing on a dry smooth surface. *Phys. Rev. Lett.* **94**, 184505 (2005).
- [20] Bird, J. C., Dhiman, R., Kwon, H.-M. & Varanasi, K. K. Reducing the contact time of a bouncing drop. *Nature* **503**, 385–388 (2013).
- [21] Liu, Y., Andrew, M., Li, J., Yeomans, J. M. & Wang, Z. Symmetry breaking in drop bouncing on curved surfaces. *Nature communications* **6** (2015).
- [22] De Ruiter, J., Lagraauw, R., Van Den Ende, D. & Mugele, F. Wettability-independent bouncing on flat surfaces mediated by thin air films. *Nature physics* **11**, 48–53 (2015).
- [23] de Gennes, P.-G., Brochard-Wyart, F. & Quéré, D. *Gouttes, Bulles, Perles et Ondes, 2nd. eds.* (Belin, Paris, 2005).
- [24] Doshi, P. *et al.* Persistence of memory in drop breakup: The breakdown of universality. *Science* **302**, 1185–1188 (2003).
- [25] Oddershede, L. & Nagel, S. R. Singularity during the onset of an electrohydrodynamic spout. *Phys. Rev. Lett.* **85**, 1234–1237 (2000).
- [26] Zeff, B. W., Kleber, B., Fineberg, J. & Lathrop, D. P. Singularity dynamics in curvature collapse and jet eruption on a fluid surface. *Nature* **403**, 401–404 (2000).
- [27] Yokota, M. & Okumura, K. Dimensional crossover in the coalescence dynamics of viscous drops confined in between two plates. *Proc. Nat. Acad. Sci. (U.S.A.)* **108**, 6395–6398; In this issue, PNAS, 108 (2011) 6337. (2011).

- [28] Jeong, J.-T. & Moffatt, H. Free-surface cusps associated with flow at low reynolds number. *J. Fluid Mech.* **241**, 1–22 (1992).
- [29] Eggers, J. Air entrainment through free-surface cusps. *Phys. Rev. Lett.* **86**, 4290 (2001).
- [30] Lorenceau, É., Restagno, F. & Quéré, D. Fracture of a viscous liquid. *Phys. Rev. Lett.* **90**, 184501 (2003).
- [31] Cohen, I. & Nagel, S. R. Scaling at the selective withdrawal transition through a tube suspended above the fluid surface. *Phys. Rev. Lett.* **88**, 074501 (2002).
- [32] Burley, R. Mechanism and mechanics of air entrainment in coating processes. *Spec. Publ. R. Soc. Chem.* **129**, 94–107 (1993).
- [33] Cohen, I., Li, H., Houglund, J. L., Mrksich, M. & Nagel, S. R. Using selective withdrawal to coat microparticles. *Science* **292**, 265–267 (2001).
- [34] Frohn, A. & Roth, N. *Dynamics of droplets* (Springer Science & Business Media, 2000).
- [35] Wilson, K. G. Feynman-graph expansion for critical exponents. *Phys. Rev. Lett.* **28**, 548 (1972).
- [36] Cardy, J. *Scaling and Renormalization in Statistical Physics* (Cambridge Univ. Press, Cambridge, 1996).
- [37] Barenblatt, G. I. *Scaling, self-similarity, and intermediate asymptotics: dimensional analysis and intermediate asymptotics*, vol. 14 (Cambridge University Press, 1996).
- [38] Chai, Y. *et al.* A direct quantitative measure of surface mobility in a glassy polymer. *Science* **343**, 994–999 (2014).
- [39] See supplemental material at [url will be inserted by publisher] for movies 1 to 4. .
- [40] Eggers, J. Theory of drop formation. *Physics of Fluids* **7**, 941–953 (1995).
- [41] Okumura, K. Viscous dynamics of drops and bubbles in hele-shaw cells: drainage, drag friction, coalescence, and bursting. *Advances in Colloid and Interface Science*; <https://doi.org/10.1016/j.cis.2017.07.021> (2017).

Figures

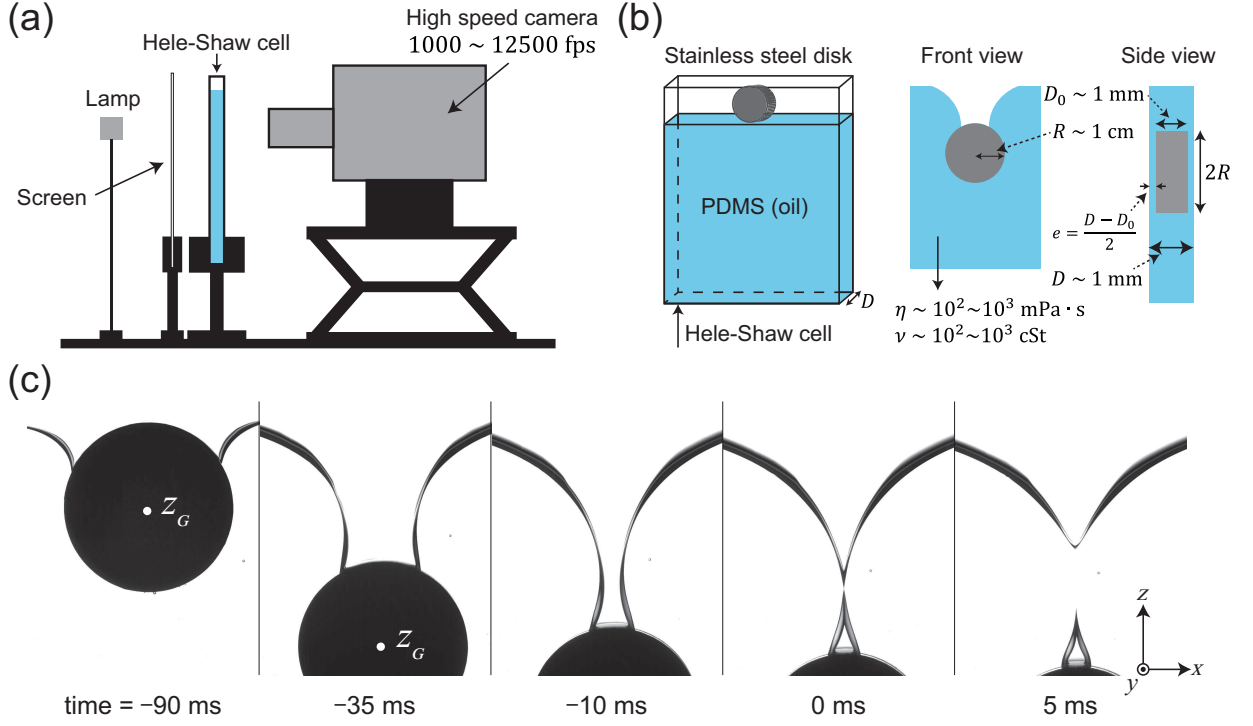


FIG. 1: (a) Experimental setup. (b) Experimental geometry. The disk of radius R with thickness D_0 falls in the Hele-Shaw cell of thickness D filled with a silicone oil of viscosity η and kinematic viscosity $\nu = \eta/\rho$ (ρ is the density of the oil). Thin oil films of thickness e exist between the surfaces of the disk and cell walls. (c) Overall pinch-off dynamics of air dragged by the disk observed from the front of the cell for $(\nu, D, R, e) = (100, 4, 10, 0.5)$ where ν is given in the unit cSt and the others are in the unit mm.

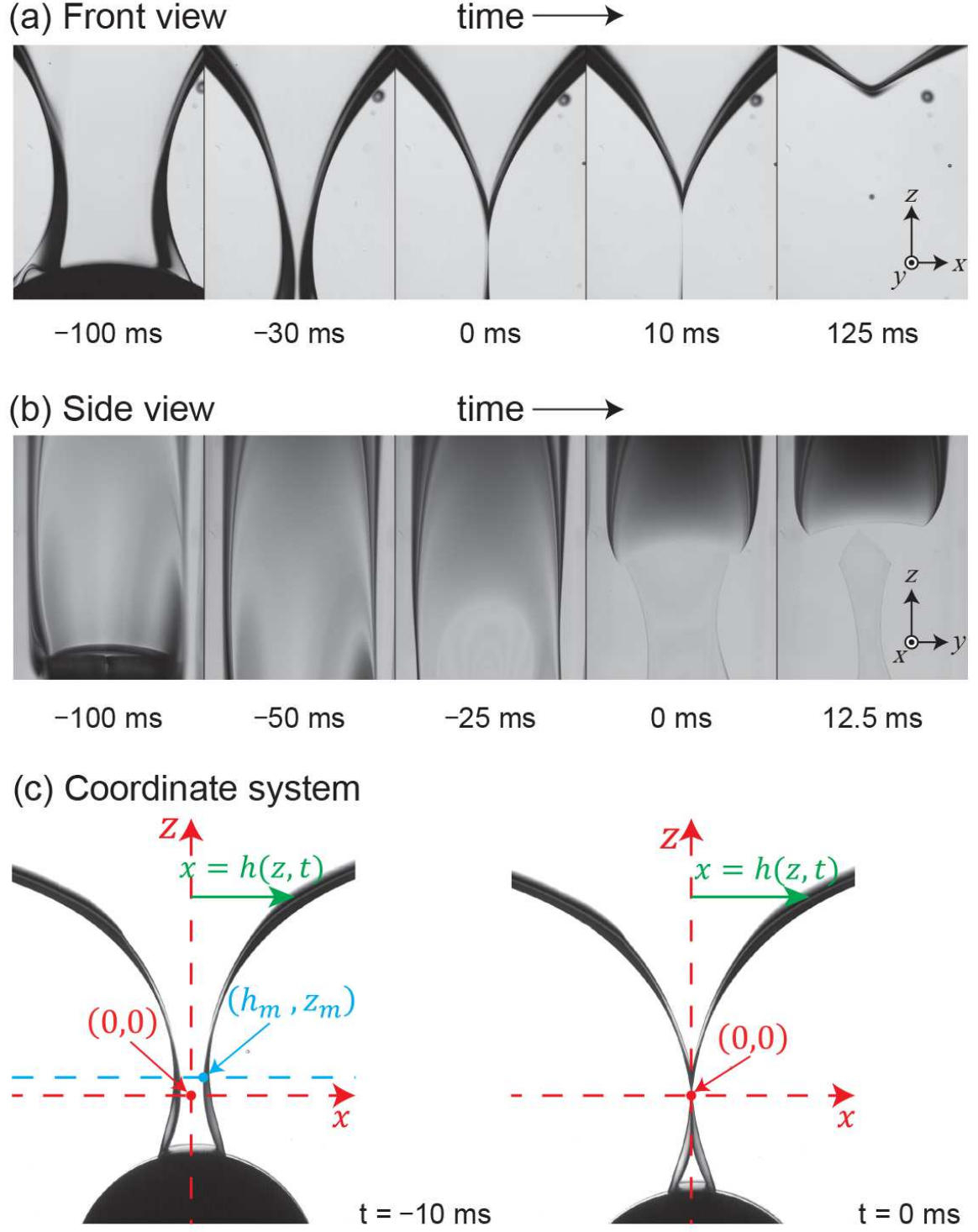
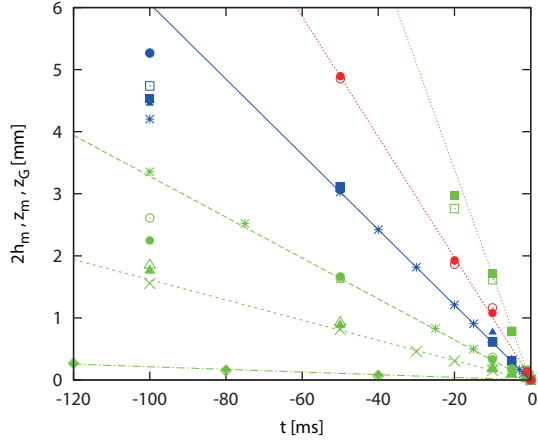
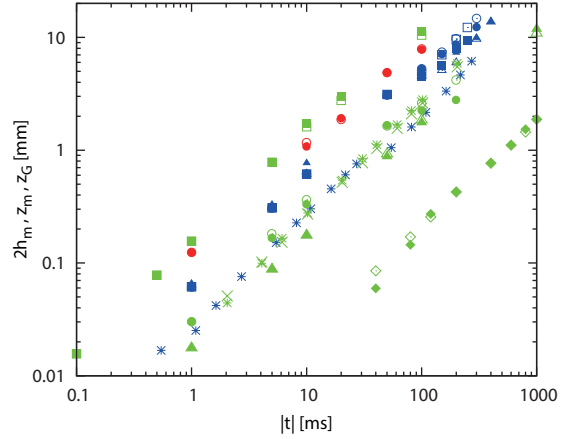


FIG. 2: Pinch-off dynamics observed from the front (a) and from the side (b) for $(\nu, D, R, e) = (500, 5, 10, 0.5)$ with the units specified in Fig. 1. (c) Definitions of geometrical parameters, the minimum neck width $2h_m$, the vertical position of the minimum neck z_m , and the neck profile $x = h(z, t)$. Snapshots are taken for $(\nu, D, R, e) = (100, 3, 10, 0.5)$.

(a) All the data on a linear scale



(b) All the data on a log-log scale



(c) All the data collapsed on a master curve

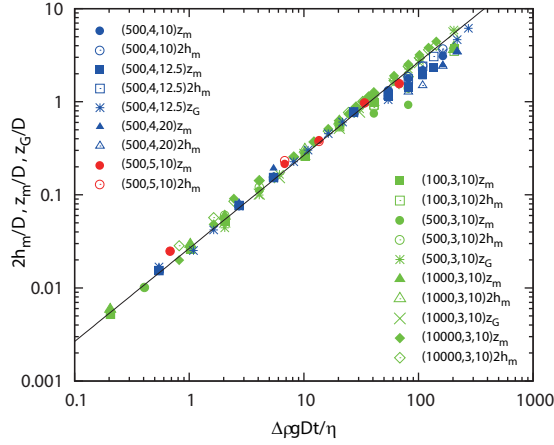


FIG. 3: The neck width $2h_m$, the vertical position of the neck z_m , and the center of mass of the disk z_G as a function of time t . (t and z_m are measured from the origins $t = t_c$ and $z = z_c$, respectively, while z_G from $z = z_G$ at $t = t_c$.) The symbols are specified in the plots by the set (ν, D, R) as in Figs. 1 and 2. (a) All the data on a linear-linear scale. (b) The same data on a log-log scale. (c) All the data collapsed on a single master line with slope one, establishing Eq. (1) with Eq. (2); the best-fitting line gives $k = 0.02764 \pm 0.00008$. The dashed lines in (a) are guide for the eye.

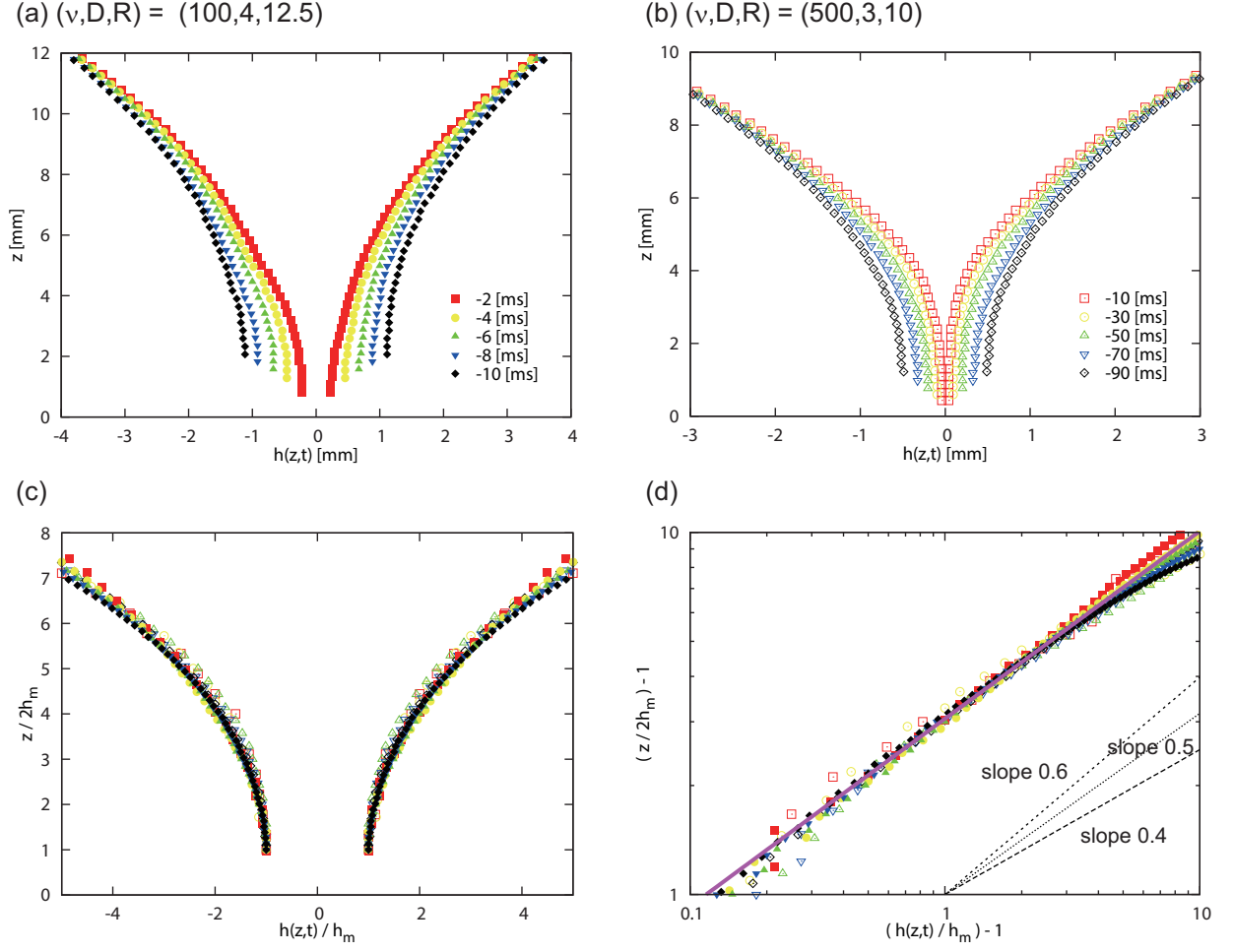


FIG. 4: Self-similar dynamics of the neck shape. (a) and (b) Neck profile $h(z, t)$ as a function of z at different times for $(\nu, D, R, e) = (100, 4, 12.5, 0.5)$ and $(500, 3, 10, 0.5)$ in the units cS and mm. (c) Profiles in (a) and (b) collapsed by rescaling with a single length scale $2h_m = z_m = l(t)$. (d) Right branches of the collapsed neck shape in (c) on a log-log scale, establishing Eq. (4) with the best-fitting line giving $a = 3.1415 \pm 0.011$.